Lawrence Berkeley National Laboratory
Chemical Sciences

Title
Electrostatic Interaction-Directed Growth of Nickel Phosphate Single-Walled Nanotubes for High Performance Oxygen Evolution Reaction Catalysts

Authors
Liu, Huiling
Li, Haoyi
Wang, Xun

Electrostatic Interaction-Directed Growth of Nickel Phosphate Single-Walled Nanotubes for High Performance Oxygen Evolution Reaction Catalysts

Huiling Liu, Haoyi Li, and Xun Wang*

Electrostatic interaction, widely existing both in natural and artificial systems, has attracted considerable research interests in nanoscience. In a system containing nanoparticles, electrostatic interaction can arise internally between charged/electric-dipolar nanoparticles/additives[1] or externally from electric field.[2] Ions, intrinsically possessing charges, usually contribute electrostatic interactions in various systems. Different ionic additives, especially halide ions, have been confirmed to be crucial to the growth of nanoparticles.[3] However, instead of electrostatic interactions, the real effects behind mainly arise from the modification of surface energy on different nanoparticles facets by absorbed ions. For the growth of nanoparticles, the study of electrostatic interactions from ions in synthetic systems still remains much unknown space. And as electrostatic force in a system can be easily tuned by many factors such as pH,[1b] ionic strength[4] or charged additives,[5] it will be a powerful way to modify such interaction for controllable synthesis of nanomaterials. Here, the electrostatic interactions from a series of alkali metal ions are utilized for controllable synthesis of nickel phosphate-based nanotubes.

The controllable synthesis of single-walled nanotubes (SWNTs) has always been of great importance.[6] A recent report on the synthesis of SWNTs provided a general growth mechanism based on the self-coiling of sub-1 nm building blocks.[7] However, the fabrication of SWNTs with tunable structure parameters still remains a great challenge. For a nanoparticle, the finally achieved structure is greatly determined by the evolution of related intermediates in growth process. And in solution growth processes, the evolutions are traditionally controlled by the manners of monomer attachment[8] (monomer attachment to nuclei) or nanoparticles attachment[1a,9] (oriented attachment). However, it has been discovered that, in some cases, intermediates could change their shapes through bending, folding or coiling themselves, making the most contribution to the formed architecture

of nanocrystals.[10] Ultrathin dimensions have been demonstrated to make nanocrystals possess low resistance to shape deformations and low resulted strain energy.[11] Thus when ultrathin structures are designed as intermediates (tiny spherical clusters are not included here), it is reasonable to speculate that their shape deformations will strongly determine the architectures of grown nanoparticles. If one-dimensional (1D) ultrathin intermediates can deform like "soft ropes" and two-dimensional (2D) ones can behave like "soft papers", it would be imaginable that their various shape deformations could result in diverse delicate architectures. While, from the point of controllable synthesis, it is of great importance to control the deformation behaviors of ultrathin intermediates. Here, we demonstrate the ability to tune the strength of electrostatic force between ultrathin intermediates and a series of alkali metal ions with different radius, for modifying the bending procedure of intermediates during the nanotube growth. Then, we can control the diameters and lengths of highly uniform single-walled nickel phosphate-based nanotubes. And except for the morphology of the nanotubes, the compositions can be flexibly changed for endowing the materials with promising electrocatalytic activity to oxygen evolution reaction. The strategy developed in this communication is believed to not only provide an effective method to enrich the family of inorganic single-walled nanotubes but also inspire the controllable design of more delicate nanostructures from special ultrathin intermediates.

The series of nickel phosphate nanotubes with different diameters and lengths were synthesized under the control of alkali metal ions, i.e., Li^+, Na^+, K^+, and Cs^+. The detailed description of the synthetic procedures is provided in the experiment section. The transmission electron microscopy (TEM) images in **Figure 1**a–d give a whole presentation of the four kinds of nanotubes. They are named nickel phosphate-Li-nanotubes (NiP_{Li}-NTs), nickel phosphate-Na-nanotubes (NiP_{Na}-NTs), nickel phospahte-K-nanotubes (NiP_K-NTs), and nickel phosphate-Cs-nanotubes (NiP_{Cs}-NTs), in sequence. Their morphology parameters are summarized in Table S1 in the Supporting Information and the corresponding size distribution is also given in Figures S1–S4 (Supporting Information). Obviously, the larger the radius of used alkali metal ion is, the narrower and longer the nanotubes are. More specifically, for NiP_{Li}-NTs and NiP_{Na}-NTs, the lengths along nanotubes axis are smaller than the diameters (Figure 1a,b); in contrast, the NiP_K-NTs and NiP_{Cs}-NTs show much longer

H. Liu, H. Li, Prof. X. Wang
Key Lab of Organic Optoelectronics
and Molecular Engineering
Department of Chemistry
Tsinghua University
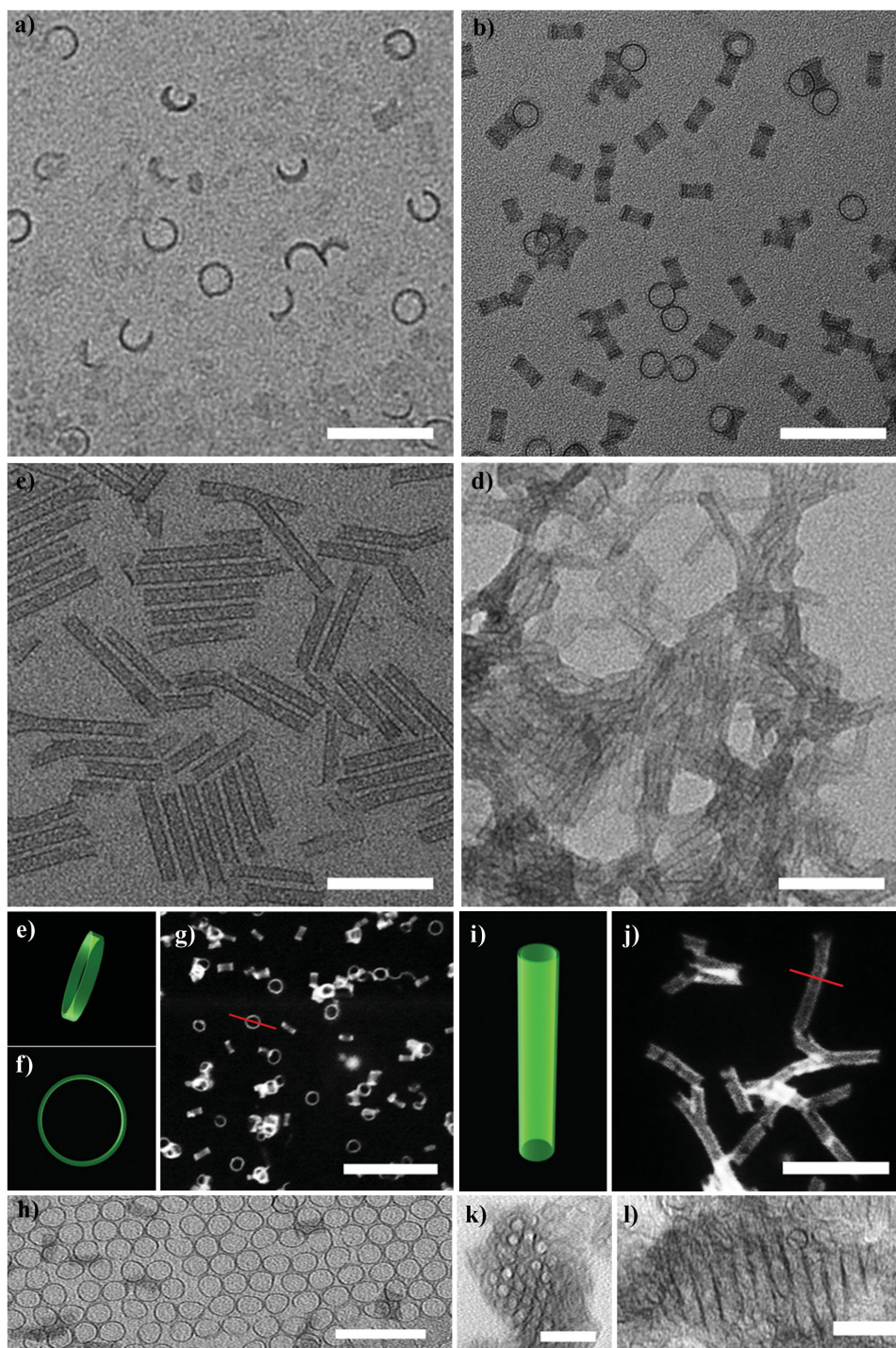Beijing 100084, China
E-mail: wangxun@mail.tsinghua.edu.cn

Figure 1. a–d) Typical TEM images of NiP$_{Li}$-NTs, NiP$_{Na}$-NTs, NiP$_K$-NTs, and Cs-NTs. Ideal models of NiP$_{Na}$-NTs along e) nanotube axis and f) lateral (radial) directions observed in panel (b). i) Model of NiP$_K$-NTs. TEM image of superlattice assembled by h) NiP$_{Na}$-NTs and NiP$_K$-NTs along k) nanotube axis and l) lateral directions. STEM images of g) NiP$_{Na}$-NTs and j) NiP$_K$-NTs, the red lines show the line-scan EDS analysis positions. Scale bar: a–d,g,j, 50 nm; h,k,l, 25 nm.

lengths but smaller diameters (Figure 1c,d). Considering the typical structures of NiP$_{Na}$-NTs and NiP$_K$-NTs, in the following discussions, these two are always selected as the representatives. It is obvious that all the nanotubes possess uniform diameters. Typically, for NiP$_{Na}$-NTs, the observation along both the axis (the corresponding model is given in Figure 1e) and radius directions (Figure 1f) in Figure 1b

shows that their uniformity exists in not only the length but also the diameter. And this is further demonstrated by the assembly behavior observed in Figure 1h, which forms regular pattern on a copper grid. As for NiP$_K$-NTs with longer length, the uniform diameter can also be highlighted by the assembled nanotubes (Figure 1k,l) formed when ethanol was added to their cyclohexane dispersion. The hollow structures

of the nanotubes are clearly presented by the dark field scanning TEM (STEM) images of NiP$_{Na}$-NTs (Figure 1g) and NiP$_{K}$-NTs (Figure 1j). The linear energy-dispersive X-ray spectra in Figure S5b,d in the Supporting Information further confirm the hollow inner by showing the greater Ni intensity at the edges of nanotubes.

To identify the chemical composition of the nanotubes, a series of characterizations including X-ray diffraction (XRD), X-ray photoelectron spectroscopy (XPS), and inductively coupled plasma (ICP) optical emission spectrometry were performed on as-prepared products. A summary of XRD results in Figure S6a in the Supporting Information exhibits the high similarity of all the patterns. Not like in some reports, where gradual XRD peak shifts exist due to the intercalation of ions with different radius into a same basic structure,[12] no obvious peak shift is observed in our case, confirming that the different alkali metal ions do not grow into the formed nanotubes. A typical pattern of NiP$_{K}$-NTs (Figure S6b) is carefully indexed to Ni$_3$(PO4)$_2$ (JCPDS card 38-1473). The broadening and some relative intensity decrease of the peaks are mainly due to the ultrathin feature of the nanotubes. The Ni 2p and P 2p core-levels are given in Figure S10 (Supporting Information), confirming the consistent Ni and P chemical states with the phase determined by XRD results.[13] And the calculation

from ICP analysis (Table S2, Supporting Information) on the ratios between Ni and P also gives values all around 1.5, i.e., the corresponding ratio in Ni$_3$(PO4)$_2$. Meanwhile, the amounts of alkali metal ions in the products before and after water washing were compared in ICP data. The trace amounts of the ions in washed samples further confirm the absence of structural alkali metal ions in the nanotubes. The relatively higher amounts of the ions in non-washed samples are derived from some absorbed salts.

To confirm that it is indeed the alkali metal cations, not other conditions, that act as the decisive factor on the controllable synthesis, a set of control experiments was performed. Again, representative NiP$_{Na}$-NTs and NiP$_{K}$-NTs systems are presented. First, the ratio between Ni and phosphate precursor amounts was varied to be higher and lower than the corresponding stoichiometric ratio (3:2) of Ni$_3$(PO$_4$)$_2$. The results in **Figure 2**a,b,e,f reveal that the basic morphologies are almost maintained and only decreased purity is observed in some cases. And considering the use of dihydrogen phosphates as precursors, the effect of pH of the synthetic systems on the nanotubes formation is also investigated. Hydrochloric acid and NaOH/KOH were selected to decrease and increase the pH value, respectively. Again, no morphology transition between the two typical classes happens (Figure 2c,d,g,h).
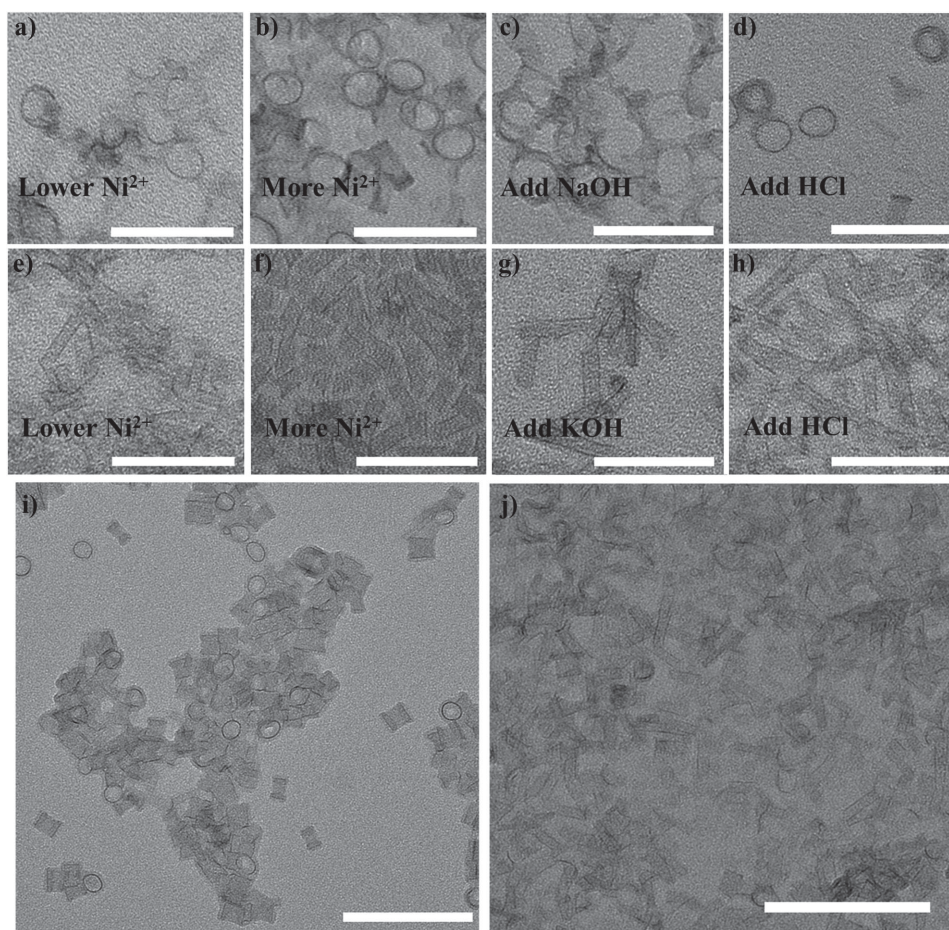

Figure 2. The influence of ratios of precursors and pH on the morphologies of synthetic a–d) NiP$_{Na}$-NTs and e-h) NiP$_{K}$-NTs. TEM images of i) NiP$_{Na}$-NTs and j) NiP$_{K}$-NTs with corresponding alkali metal chlorides (NaCl and KCl) and phosphoric acid, showing the effectiveness of used alkali metal ions. Scale bar: a–h, 50 nm; i,j, 100 nm.

Interestingly, the structures keep very well under low pH but are respectively sensitive to high pH. Actually, the influence of reaction temperature, the composition of involved solvents, and the amount of water on the morphology of the nanotubes have also been investigated and exhibited in Figures S7–S9 in the Supporting Information. The morphology of the nanotubes seems to be robust and not sensitive to the controlled parameters. Based on this, we tend to propose that the surfactants in our case act as the capping ligands for confining the size of the ultrathin preformed structures rather than forming cylindrical soft templates. The structures of soft templates are usually sensitive to reaction conditions. To further give direct evidence, the combination of phosphoric acid (H_3PO_4) and NaCl/KCl is designed to replace the corresponding alkali metal phosphates. It is clearly demonstrated by the TEM images in Figure 2i,j that the typical NiP_{Na}-NTs and NiP_K-NTs can also be successfully constructed through the exchanged reaction sources, directly confirming the essential role of the alkali metal ions. When the mixture of sodium and potassium dihydrogen phosphates is utilized, two typical nanotubes coexist in Figure S11 in the Supporting Information.

Once the role of alkali metal ions is confirmed, we move forward to try to provide a reasonable explanation on how the ions influence the morphology parameters of the nickel phosphate nanotubes. We have found that the formation of nanotubes is initiated by the self-coiling of ultrathin building blocks under proper weak interactions.[7] The building blocks formed at early stage refer to the tiny nanosheets in Figures S12a and S13a in the Supporting Information, and their ultrathin feature of sub-1 nm thickness can be observed through the lateral surface of some curved nanosheets. More careful tracking to the growth evolution of NiP_{Na}-NTs and NiP_K-NTs is provided in Figures S12 and S13 in the Supporting Information. Electrostatic interaction, which has been widely applied in molecular and nanoparticles assembly, may be the main function from the ions to tune the behaviors of ultrathin building blocks. Based on the electrostatic force equation

$$F = \frac{q_1 q_2}{4\pi\varepsilon_0\varepsilon_r}\frac{1}{r^2}$$

where q = charge, ε_0 = permittivity of free space, ε_r = dielectric constant of surrounding material, r = distance between charged particles, the interaction between ions from Li^+ to Cs^+ and the building blocks decreases, where the ions possess the same charge number but gradually increased radius. It means that the electrostatic attraction of Li^+ is the strongest and the attraction of Cs^+ is the weakest relatively. This may lead to a highest density of attracted Li^+ on the surfaces of ultrathin building blocks in NiP_{Li}-NTs system and a lowest value in NiP_{Cs}-NTs case. It is obvious that, in our case, the bending process during the self-coiling of the ultrathin building blocks greatly affects the finally formed nanotubes. If the bending is approximately treated as the simplest case of plate bending, the flexural rigidity (D) of the building blocks can be expressed as $D = Et^3/12(1-\mu^2)$, where E is the Young modulus, t is the thickness of a plate,

μ is the Poisson ratio. Based on the above considerations, the building blocks with high attracted density of Li^+ may possess high E, leading to high D which makes the bending difficult. And the difficulty results in a large diameter with small curvature. By parity of reasoning, the level of the bending difficulty gradually decreases from NiP_{Li}-NTs system to NiP_{Cs}-NTs system, making the resulting diameter decrease and curvature increase (**Figure 3**). What's more, the attraction of the ions may also bring extra charges on the building block surface. Stronger attraction usually leads to more extra charges remained on the surface, making the repulsive force among the building block units stronger and the related bending more difficult. This probably also makes a contribution to the gradual decrease of the diameter from NiP_{Li}-NTs to NiP_{Cs}-NTs. On the other hand, strong attraction probably hinders the diffusion of precursors to grow on the coiled building blocks, gives short $NiP_{Li/Na}$-NTs and long $NiP_{K/Cs}$-NTs. Interestingly, as illustrated by the former XRD and ICP results, the alkali metal ions do not grow into the nanotube structures, which reveals that the electrostatic interaction discussed here is relatively weak at a whole level.

Besides the control of morphology parameters on the nanotubes, the compositions can also be varied through doping Co and Fe. Figure S14a,b (Supporting Information) shows that the morphologies of NiP_{Na}-NTs and NiP_K-NTs are well maintained after doping Co (named nickel phosphate(Co)-Na-nanotubes (NiP_{Na} (Co)-NTs) and nickel phosphate(Co)-K-nanotubes (NiP_K (Co)-NTs)). And co-doping of Co and Fe into NiP_{Na}-NTs with different doping levels can also be achieved (named nickel phosphate(Co_3Fe_1)-Na-nanotubes ($NiP_{Na}(Co_3Fe_1)$-NTs) and nickel phosphate(Co_2Fe_2)-Na-nanotubes ($NiP_{Na}(Co_2Fe_2)$-NTs)). (Figure S14c,d, Supporting Information) The doped Co and Fe for all are confirmed to be Co^{2+}[14] and Fe^{3+},[15] respectively, based on their 2p core-levels in Figure S15 in the Supporting Information. Linear-scan energy-dispersive X-ray (EDX) data of a single $NiP_{Na}(Co_2Fe_2)$-NTs and element mapping data across several assembled $NiP_{Na}(Co_2Fe_2)$-NTs in Figures S16 and S17 in the Supporting Information both show that Co and Fe ions are uniformly co-doped into NiP_{Na}-NTs. And ICP characterization is conducted to give accurate doping amounts and the results are provided in Table S3 in the Supporting Information.
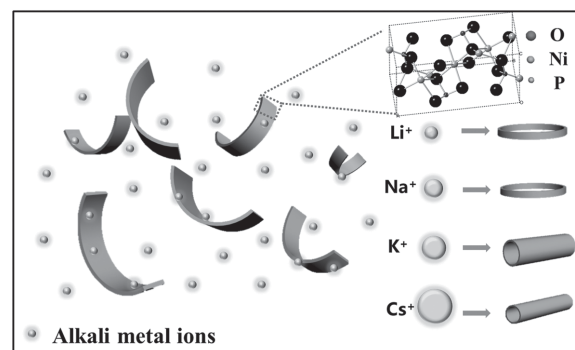

Figure 3. Scheme for the formation of single-walled nickel phosphate nanotubes with controllable structural parameters under the utilization of a series of alkali metal ions.

3d-M metal (M = Ni, Co, Fe, Mn) based compounds have been demonstrated to possess promising electrochemically catalytic activity to oxygen evolution reaction (OER) in alkaline environments.[16] The nickel phosphate-based nanotubes reported here are expected to exhibit desirable properties. We therefore investigated the OER catalytic performances of the as-synthesized nanotubes in O_2 saturated 1 M KOH solution. Linear sweep voltammetry was applied on the samples to confirm their overpotentials (η_{10}) for achieving 10 mA cm^{-2} current density, which is the demand for a 10% efficient solar-to-fuel conversion device.[17] As shown in **Figure 4**a, nickel phosphate nanotubes (NiP$_K$-NTs as the representative) without doping show low current density over the full range of applied potentials, which means their poor catalytic activity. However, after doping with Co, both NiP$_{Na}$(Co)-NTs and NiP$_K$(Co)-NTs show apparently increased current densities, with η_{10} of 400 and 420 mV, respectively. Remarkably, the current densities further increase and the overpotentials shift to be less positive when co-doping of Co and Fe is performed on NiP$_{Na}$-NTs. The lowest overpotential owned by NiP$_{Na}$(Co$_2$Fe$_2$)-NTs is 300 mV which is 40 mV lower than that of NiP$_{Na}$(Co$_3$Fe$_1$)-NTs. At the same potential (overpotential η = 0.35 V), the current density of NiP$_{Na}$(Co$_2$Fe$_2$)-NTs is confirmed to be approximately 14-fold higher than that of NiP$_K$(Co)-NTs (Figure 4b). To confirm whether the high current of NiP$_{Na}$(Co$_2$Fe$_2$)-NTs arises from pure OER, Faradaic efficiency of this typical nanotubes is measured and given in Figure S18 in the Supporting Information. The highest efficiency is ≈90%. While it is a little lower than some reported values, the value is acceptable. After doping Fe into NiP$_{Na}$(Co)-NTs, the observed oxidation peaks appearing before the onset potential of OER obviously move positively. XPS data of NiP$_{Na}$(Co$_2$Fe$_2$)-NTs after OER measurement in

Figure S19 in the Supporting Information show the existence of Co^{3+} and Ni^{3+}, indicating that the redox processes contain the redox of Co(II)/Co(III) and Ni(II)/Ni(III). For Ni film containing Fe, some reports have stated that the existence of Fe can resist the redox of Ni compounds and result in a positive move of the redox peaks. And more amount of Fe results in higher level of positive move and better OER performance.[18] In our case, the similar result is possibly due to the same reason. The Tafel slopes of the series of samples are summarized in Figure 4c. Samples co-doped with Co and Fe give out the slopes of ≈55 mV dec^{-1}. Based on these results, it is absolutely confirmed that doping Fe can greatly promote the OER activity of the nanotubes. It has been demonstrated that Fe can enhance the OER performance of nickel-based nanomaterials.[19] In our case, the ultrathin feature of the nanotubes and available inner and outer surfaces result in extremely high exposed surface atoms, further facilitating the contact of electrolytes with Fe-promoted catalysts surfaces. Brunauer-Emmett-Teller (BET) data of the Nickel phosphate-based nanotubes are provided in Table S3 in the Supporting Information. All the nanotubes based on NiP$_{Na}$-NTs (e.g., NiP$_{Na}$(Co)-NTs, NiP$_{Na}$(Co$_3$Fe$_1$)-NTs, NiP$_{Na}$(Co$_2$Fe$_2$)-NTs) with similar diameter and length possess similar surface area. The NiP$_K$(Co)-NTs with higher length show a lower surface area. Figure S20 (Supporting Information) further gives the OER activity based on the surface area. The tested samples were all mixed with carbon powder, which has been demonstrated to be an effective and simple method to enhance the conductivity of the mixed system.[20] Electrochemical impedance results (Figure S20a,b, Supporting Information) clearly confirm the consistent decreasing of charge transfer resistance after carbon mixing. The compared LSV and Tafel results of samples with and
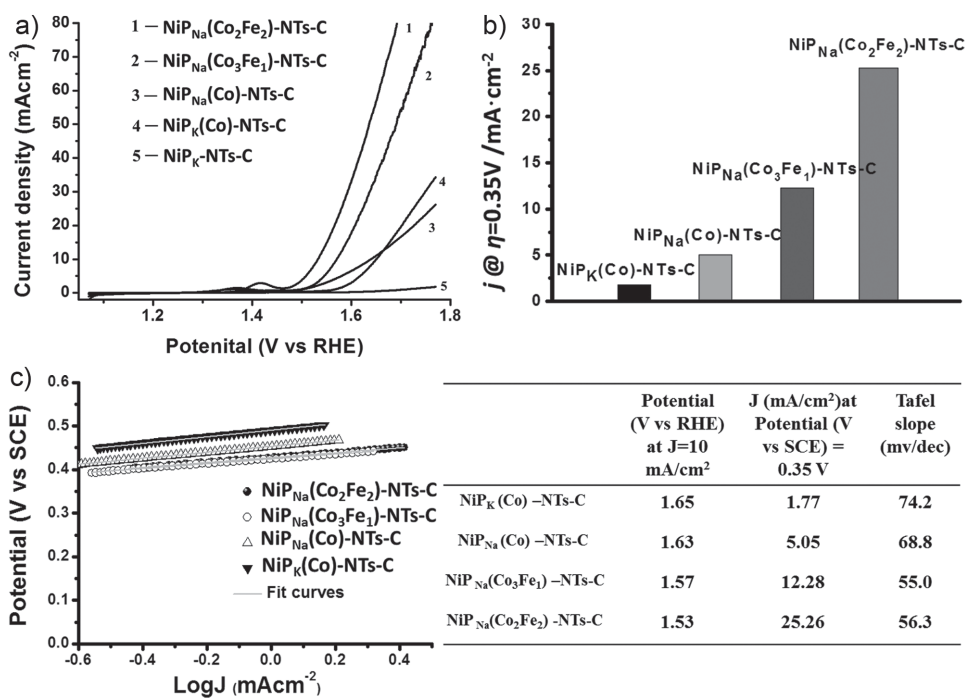

	Potential (V vs RHE) at J=10 mA/cm²	J (mA/cm²) at Potential (V vs SCE) = 0.35 V	Tafel slope (mv/dec)
NiP$_K$(Co) –NTs-C	1.65	1.77	74.2
NiP$_{Na}$(Co) –NTs-C	1.63	5.05	68.8
NiP$_{Na}$(Co$_3$Fe$_1$) –NTs-C	1.57	12.28	55.0
NiP$_{Na}$(Co$_2$Fe$_2$) -NTs-C	1.53	25.26	56.3

Figure 4. a) Polarization curves of compared samples with different doped ions and levels (scan rate of 1 mV s^{-1}). b) Current density of the series of catalysts at an overpotential of 0.35 V. c) Tafel plots of doped nanotubes.

without carbon addition directly demonstrate the effectiveness of added carbon (Figure S9c,d, Supporting Information). Test on stability of $NiP_{Na}(Co_3Fe_1)$-NTs and $NiP_{Na}(Co_2Fe_2)$-NTs is provided in Figure S22 in the Supporting Information.

In summary, nickel phosphate single-walled nanotubes with tunable structure parameters have been fabricated under the control of a series of alkali metal ions including Li^+, Na^+, K^+, and Cs^+. Different strengths of electrostatic interaction between the ions and the early-stage formed ultrathin building blocks are proved to influence the bending behaviors of the blocks, therefore determining the resulted diameters and lengths of the nanotubes. Besides the controllable structures, the universal of the developed strategy endows the doping of Co and Fe into the nanotubes to improve their OER performances. We expect our endeavor made here could inspire the synthesis of tunable inorganic single-walled nanotubes for promoting the development of such important nanomaterials. More significantly, it is believed that this work will further the study for fabricating delicate nanostructures based on interesting ultrathin building blocks.

Experimental Section

NiP_Li-NTs and NiP_Na-NTs: In a typical synthesis, 3 mL ethanol and 3 mL cyclohexane were mixed with the mixture of 1.62 g oleyamine (OAm) and 0.89 g oleic acid in a 10 mL-Teflon autoclave to form a homogeneous solution. Then with vigorous stirring, 0.3 mL $NiCl_2$ aqueous solution (10 M) and 0.2 mL LiH_2PO_4/NaH_2PO_4 aqueous solution (10 M) was added into the autoclave in sequence. After stirring for 10 min, the autoclave was sealed and heated at 160 °C for 8 h. After cooling down to around 30 °C, the product at the bottom of autoclave was dispersed in 10 mL cyclohexane, and then precipitated with the addition of 20 mL ethanol and centrifuged at 8000 rpm for 5 min to remove the excess surfactants. After three cycles of dispersion and centrifugation wash, green product was dispersed in cyclohexane.

NiP_K-NTs: For the synthesis of NiP_K-NTs, the procedure is the same as that of $NiP_{Li/Na}$-NTs, except 6 mL ethanol was used to replace the mixture of 3 mL ethanol and 3 mL cyclohexane in the synthetic system.

NiP_Cs-NTs: Based on the synthesis of NiP_K-NTs, only the precursor of phosphate was modified by using 0.2 mL CsCl aqueous solution (10 M) and 11 μL pure H_3PO_4 (2 mmol).

Doped NTs: Corresponding amounts of $CoCl_2$ and $FeCl_3$ aqueous (10 M) were utilized, together with $NiCl_2$ aqueous, to dope cobalt and iron ions into the NTs.

Supporting Information

Supporting Information is available from the Wiley Online Library or from the author.

[1] a) K. S. Cho, D. V. Talapin, W. Gaschler, C. B. Murray, *J. Am. Chem. Soc.* **2005**, *127*, 7140; b) R. A. French, A. R. Jacobson, B. Kim, S. L. Isley, R. L. Penn, P. C. Baveye, *Environ. Sci. Technol.* **2009**, *43*, 1354; c) H. Zhang, D. Wang, *Angew. Chem. Int. Ed.* **2008**, *120*, 4048.

[2] K. M. Ryan, A. Mastroianni, K. A. Stancil, H. Liu, A. Alivisatos, *Nano Lett.* **2006**, *6*, 1479.

[3] a) M. Chen, B. Wu, J. Yang, N. Zheng, *Adv. Mater.* **2012**, *24*, 862; b) S. E. Lohse, N. D. Burrows, L. Scarabelli, L. M. Liz-Marzán, C. J. Murphy, *Chem. Mater.* **2013**, *26*, 34.

[4] J. Kolny, A. Kornowski, H. Weller, *Nano Lett.* **2002**, *2*, 361.

[5] K. A. Huynh, K. L. Chen, *Environ. Sci. Technol.* **2011**, *45*, 5564.

[6] a) R. Tenne, L. Margulis, M. Genut, G. Hodes, *Nature* **1992**, *360*, 444; b) N. G. Chopra, R. Luyken, K. Cherrey, V. H. Crespi, M. L. Cohen, S. G. Louie, A. Zettl, *Science* **1995**, *269*, 966; c) M. Remskar, A. Mrzel, Z. Skraba, A. Jesih, M. Ceh, J. Demšar, P. Stadelmann, F. Lévy, D. Mihailovic, *Science* **2001**, *292*, 479.

[7] B. Ni, H. Liu, P. P. Wang, J. He, X. Wang, *Nat. Commun.* **2015**, *6*, 8756.

[8] Y. Yin, A. P. Alivisatos, *Nature* **2005**, *437*, 664.

[9] A. Halder, N. Ravishankar, *Adv. Mater.* **2007**, *19*, 1854.

[10] a) F. Saleem, Z. Zhang, B. Xu, X. Xu, P. He, X. Wang, *J. Am. Chem. Soc.* **2013**, *135*, 18304; b) X. Y. Kong, X. Ding, R. Yang, Z. L. Wang, *Science* **2004**, *303*, 1348.

[11] a) S. Hu, H. Liu, P. Wang, X. Wang, *J. Am. Chem. Soc.* **2013**, *135*, 11115; b) P. P. Wang, Y. Yang, J. Zhuang, X. Wang, *J. Am. Chem. Soc.* **2013**, *135*, 6834; c) J. He, H. Liu, B. Xu, X. Wang, *Small* **2015**, *11*, 1144.

[12] a) A. Ookubo, K. Ooi, F. Tani, H. Hayashi, *Langmuir* **1994**, *10*, 407; b) M. R. Lukatskaya, O. Mashtalir, C. E. Ren, Y. Dall'Agnese, P. Rozier, P. L. Taberna, M. Naguib, P. Simon, M. W. Barsoum, Y. Gogotsi, *Science* **2013**, *341*, 1502.

[13] D. Siconolfi, R. Frankenthal, *J. Electrochem. Soc.* **1989**, *136*, 2475.

[14] K. Yu, B. B. Zhou, B. Yu, Z. H. Su, G. Y. Yang, *Inorg. Chem.* **2011**, *50*, 1862.

[15] L. Castro, R. Dedryvere, M. El Khalifi, P. E. Lippens, J. Breger, C. Tessier, D. Gonbeau, *J. Phys. Chem. C* **2010**, *114*, 17995.

[16] a) R. Subbaraman, D. Tripkovic, K. C. Chang, D. Strmcnik, A. P. Paulikas, P. Hirunsit, M. Chan, J. Greeley, V. Stamenkovic, N. M. Markovic, *Nat. Mater.* **2012**, *11*, 550; b) M. W. Kanan, D. G. Nocera, *Science* **2008**, *321*, 1072; c) A. J. Esswein, Y. Surendranath, S. Y. Reece, D. G. Nocera, *Energy Environ. Sci.* **2011**, *4*, 499; d) S. M. Barnett, K. I. Goldberg, J. M. Mayer, *Nat. Chem.* **2012**, *4*, 498; e) K. Jin, J. Park, J. Lee, K. D. Yang, G. K. Pradhan, U. Sim, D. Jeong, H. L. Jang, S. Park, D. Kim, *J. Am. Chem. Soc.* **2014**, *136*, 7435; f) A. Bergmann, I. Zaharieva, H. Dau, P. Strasser, *Energy Environ. Sci.* **2013**, *6*, 2745; g) M. Wiechen, I. Zaharieva, H. Dau, P. Kurz, *Chem. Sci.* **2012**, *3*, 2330; h) K. Jin, A. Chu, J. Park, D. Jeong, S. E. Jerng, U. Sim, H. Y. Jeong, C. W. Lee, Y. S. Park, K. D. Yang, *Sci. Rep.* **2015**, *5*, 10279.

[17] C. C. McCrory, S. Jung, J. C. Peters, T. F. Jaramillo, *J. Am. Chem. Soc.* **2013**, *135*, 16977.

[18] M. W. Louie, A. T. Bell, *J. Am. Chem. Soc.* **2013**, *135*, 12329.

[19] D. Friebel, M. W. Louie, M. Bajdich, K. E. Sanwald, Y. Cai, A. M. Wise, M. J. Cheng, D. Sokaras, T. C. Weng, R. Alonso-Mori, *J. Am. Chem. Soc.* **2015**, *137*, 1305.

[20] B. Ni, X. Wang, *Chem. Sci.* **2015**, *6*, 3572.